Unsteady Analysis of a Generic Non-Axisymmetric Hub Endwall Contour as Applied to a Rotating Turbine at On and Off-Design Conditions

DI Dunn[a], TW von Backström[b], GC Snedden[c]

Received 23 August 2018, in revised form 27 November 2018 and accepted 11 December 2018

Abstract: Numerous researchers have investigated various techniques to reduce loss in gas turbine engines. One such technique that has shown promise is endwall secondary flow control using non-axisymmetric endwall contouring. Previous steady state investigations have shown that the generic endwall contour designed for a cascade reduced the loss in a rotating turbine test rig. The current investigation was to determine if there were unsteady effects introduced by the contour at design and off design conditions. An experimental and numerical study was performed to investigate the rotor flow field for any unsteady changes to the rotor exit flow field. The investigation was performed at an increased loading condition, design and a decreased loading condition to determine how changes in operating condition altered the flow field. The experimental results showed that the velocity magnitude of the hub endwall secondary flow vortex system for the contoured rotor was reduced. The peak difference in oscillation of the flow was also reduced. The effect of the endwall contour reduced the over and under turning of the endwall secondary flow vortex system as well. The magnitude of the FFT at the blade passing frequency was reduced below midspan.

Additional keywords: Non-axisymmetric endwalls, unsteady, secondary flow.

Nomenclature

Roman

y^+	Dimensionless wall distance [-]
C,V	Absolute velocity [m/s]
S	Span [mm]
W	Relative velocity [m/s]

Greek

α	Absolute yaw angle [°]
ϕ	Flow Coefficient [-]

Subscripts

mag	Magnitude
t	Tangential
x	Axial
3	Rotor outlet
stage	From stator inlet to rotor outlet

a. CSIR DPSS, Pretoria, South Africa. ddunn@csir.co.za
b. SAIMechE Honorary Fellow, Department of Mechnical and Mecatronic Engineering, Stellenbosch University.
c. CSIR DPSS, Pretoria, South Africa.

1 Introduction

Loss reduction techniques have become increasingly important in gas turbine engines in an effort to reduce operating costs as well as reduce emissions. Endwall contouring is a method that has shown promise. The current investigations are a result of works originally started by Rose [1] who found endwall contouring to be beneficial. During cascade tests Ingram [2] showed that secondary flow in a cascade could be altered by changing the passage vortex strength by non-axisymmetric endwall contouring. Snedden *et al.* [3] showed that a generic endwall contour from a cascade could be successfully implemented in a rotating turbine as a means of controlling the secondary losses. Secondary flows and the associated losses have been shown by several researchers [4,5] to exist. The main vortical structures can be seen in figure 1.

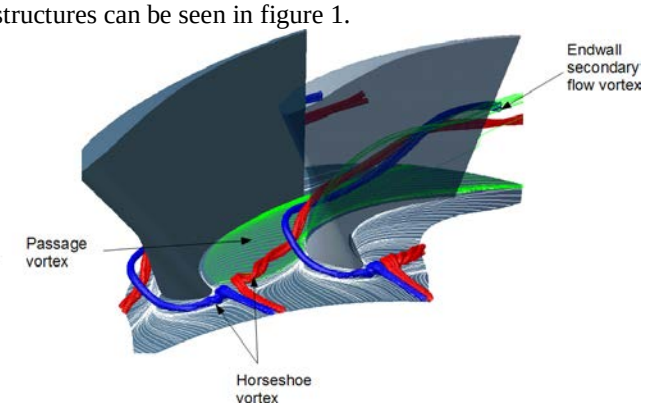

Figure 1 Image showing some of the main flow features in an endwall secondary flow system

Over the years many researchers have investigated non-axisymmetrical endwall contours. Rose *et al.* [1] used end-wall contouring to remove circumferential non-uniformities in static pressure downstream of a NGV trailing edge. Gregory-Smith *et al.* [6] designed and tested an endwall that was suitable for a real turbine. Harvey *et al.* [7] investigated how non-axisymmetric endwalls perform when used on the intermediate pressure turbine model rig for the Rolls-Royce Trent 500 engine and found the stage efficiency increased by 0.9% ± 0.4%.

Understanding how the non-axisymmetric endwalls alter the flow in and downstream of the blade row of interest is important to help design appropriate endwalls. To this end many researchers perform linear cascade test to validate endwall designs. Mensch and Thole [8] have gone as far as investigating the effect of non-axisymmetric endwall contouring and film cooling on the passage flow field. Rezasoltani *et al.* [9] (and Schobeiri *et al.* [10]) took the

research further and included the effect of purge flows in a rotating turbine.

The current investigation is a continuation of work done by Ingram [2], who designed and tested a series of non-axisymmetric endwall contours for use with the Durham linear cascade, [2]. Snedden [11] adapted the most promising of the cascade endwalls (the P2 endwall) and performed a steady state analysis in a rotating turbine test rig. The current investigation extends the previous research to include an unsteady analysis of the rotor exit flow field that has a non-axisymmetric hub endwall contour. Numerical and experimental results for three loading conditions were examined, namely design loading, increased and decreased loading (which presents with a positive and negative incidence angle). Previous publications dealt with the design and the off design cases separately, the current investigation looks at all the results together to determine if a trend is evident.

2 Experimental Setup

The experimental tests were performed using the same vertical axis 1 ½ stage turbine test rig used by Snedden *et al.* [3] and Dunn *et al.* [12], shown in figure 2. Figure 3 shows a cross section of the test section showing the relevant nomenclature. All the results presented were taken downstream of the rotor (X3 in figure 3). The test rig design summary can be seen in Snedden *et al.* [3] and Dunn *et al.* [12]. The rotor speeds and their designations used for testing can be seen in table 1.

Figure 2 Picture of the turbine test rig

The blade profile at the hub was constrained to match that of Ingram [13] to facilitate adaptation of the cascade hub endwall contour, the adapted endwall is shown in Snedden *et al.* [3]. The blades were designed by the inverse design method [14]. Refer to Snedden *et al.* [15] for a more in-depth description of the test rig.

Table 1 Rotor speeds used for testing

Test Case	Rotor Speed (RPM)	Incidence Angle (°)
Increased loading	1907	+5°
Design loading	2300	0°
Decreased loading	2820	−5°

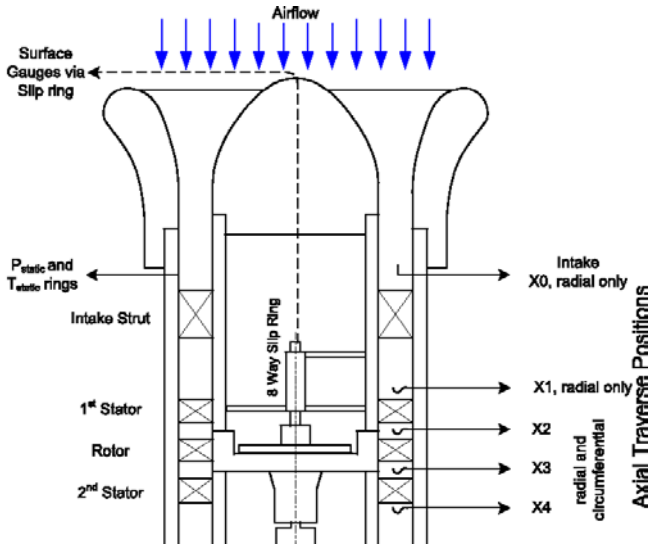

Figure 3 Schematic of the test section of the 1½ stage turbine test rig

3 Experimental Technique

Unsteady flow mapping was performed using TSI's IFA300 hotfilm system, sampling at 100 kHz (or ±130× the design blade passing frequency). Due to space constraints only a 2 component cross flow probe could be used for testing, namely the TSI's 1240 Standard Cross Flow "X" Probe. Calibrations were performed using the TSI Model 1129 auto calibrator. The auto calibrator steps through a series of predetermined air velocities (which are controlled by a computer controlled valve) and records the probe voltages. King's Law was chosen for curve fitting as it had a consistently lower mean squared error over the calibration range.

The measurement region consisted of 342 planar sample points, 18 in the tangential direction (at 1° increments) and 19 in the radial direction, starting at 3.5 mm from the hub endwall, moving out in increments of 3.1 mm. 64k samples (the IFA300 interprets this to 65536 samples) were taken at each measurement location. The data was then Phase Lock Averaged (PLA) [16,17], to facilitate with ambient noise reduction. To simplify PLA, a step wave was sampled simultaneously with the two components of the "X" probe. A step was generated after each full rotor revolution, with the first rise of the step wave being used as the reference.

The FFTs presented were taken of the raw data (all 65536 unfiltered samples), and not the phase lock averaged data. The intention was to prevent the elimination of potentially interesting frequencies (ambient noise would be consistent). The raw data was processed such that the start and end of the data set were at the same phase with respect to the rotor location (i.e. a rectangular window was used for processing).

Velocity magnitude was calculated as follows:

$$C_{mag} = \sqrt{C_x^2 + C_t^2}$$

Where C_x is axial velocity and C_t is the tangential velocity. The yaw angle was calculates using:

$$\alpha = \text{atan}(\frac{C_x}{C_t})$$

4 Numerical Setup

The numerical work presented was an extension of previous work (more detail in [18,19,20]) and for brevity was only summarised below. The simulations were performed using Numeca's FINE^{TM}/Turbo v8 [21]. FINE^{TM}/Turbo uses EURANUS as the solver which uses Runga-Kutta central and upwind differencing [21]. To facilitate the density based solver in the low Mach Number regime, Merkle pre-conditioning was used. Domain scaling with a dual time stepping technique was used for the unsteady simulations, imposing the constraint that the periodicities of the consecutive blade rows had to be equal. Thus 3 inlet stator blades, 2 rotor blades and 3 outlet stator blades (to suit the blade numbers). The SST k − ω turbulence model, as used by Snedden *et al.* [3] and Dunn *et al.* [20], was used for the simulations. Of all the turbulence models available in FINE^{TM}/Turbo it gave the best results for the current investigations. All of the turbulence models tested and chosen from can be seen in [18]. Transition modelling was investigated but found to have negligible change to the rotor exit flow field. Inclusion of intermittency modelling was found to perform worse than the transition modelling alone (more detail is provided in [18]). The mesh had approximately 5 million hexahedral cells with an average y+ < 1. Snedden [11] performed a grid dependence study and found the solution to be independent of mesh.

5 Results

For brevity only the velocity magnitude experimental results will be presented, for the tangential and axial velocity refer to [12] or [22]. The velocity magnitude was the vector sum of the measured quantities (done at each discrete time step) and was thus felt to be representative of both the axial and tangential velocities and fluctuations thereof. It should be noted that the velocity magnitude presented does not contain the radial velocity component since it could not be measured. The horizontal error bands on the unsteady velocity profiles show the range of velocities measured (minimum and maximum values). The FFT data was plotted on the same set of axes as the velocity magnitude, but use the secondary X-axis at the top of the graphs, the vertical scale of the FFT's can be found on the bottom right. The scale of the X-axis is in multiples of blade passing frequency (design loading case: 766.67 Hz, increased loading case: 635.67 Hz, and decreased loading case 940 Hz). In all cases "improvement" or "improved" should be taken to mean that the flow is more aligned in magnitude and/or trend to the design flow conditions. "Spanwise location" was measured from the hub (0% span) to the casing (100% span). The overlaid contours represent the ensemble averaged data that was used to generate the velocity profiles in the underlying plots.

5.1 Design Operating Condition

Comparing the velocity magnitude in figure 4a to figure 4b it can be seen that the flow in the endwall secondary flow region has been improved (i.e. the velocity magnitude was reduced bringing the measured value closer to design), the peak at 31% span was reduced by 2 m/s, producing a more uniform velocity profile. The variation in velocity was also reduced, however the tip region showed an increase in the variation of the velocity magnitude. The tip leakage flow also increased in magnitude for the contoured case.

The dominant frequency for all tests was the blade passing frequency, with all other frequencies of interest being the harmonics thus the contouring has not changed the overall frequency domain. In general the FFT's, shown in figure 4 (the grey horizontal lines) show a decrease in the magnitude of the fluctuating component at the blade passing frequency below 50% span, with the exception of 10% span where the magnitude increased significantly as shown in figure 5.

Comparison of the numerical results with the experimental results in figure 6 show a reasonable correlation. The regions showing the worst correlation were in regions of high shear. This is consistent with what was found by Dunn *et al.* [18] and Snedden [11] for the steady state results. Figure 6 shows that the overturning of the flow in the endwall secondary flow region was reduced by the contoured endwall. The resulting reduction in under-turning reduced the peak velocity magnitude at 31% span. The amount of under-turning at 31% span was also reduced (relative yaw angle was increased).

The stream tube in figure 7 shows that the contoured endwall secondary flow vortex structure was more radially distributed, with the suction surface leg of the contoured rotor horse shoe vortex unwrapped by comparison. This can be attributed to the reduction in strength of the cross passage pressure gradient, as intended by the design of the contour [13]. The tip leakage flow streamlines for the annular and contoured case show negligible differences. The tip leakage flow meets the endwall secondary flow vortex at midspan producing a flat contour. This suggests that for a larger blade aspect ratio the hub endwall secondary flow vortex could unwrap more creating a better midspan velocity profile.

5.2 Increased Loading Condition

The velocity magnitude in figure 8 shows that the contoured rotor has a lower peak velocity magnitude in the hub endwall secondary flow region. The peak seen in the annular case at 31% span (V_{mag} = 37.3 m/s) was reduced by 2.9 m/s and the location of peak velocity magnitude was moved radially down to 26% span for the contoured rotor. The magnitude of the fluctuations in the hub endwall secondary flow region have been reduced, except at 5.7% span where it increased. As seen with the design speeds above the magnitude of the tip leakage flow was strengthened, with the fluctuation in the flow increasing as well. As was seen in the design loading case, the contoured rotor has reduced the over-turning of the flow below 30% span, shown in figure 9. The resulting relative yaw angle being closer to design. The contoured rotor relative velocity magnitude was slightly lower in the hub region as well.

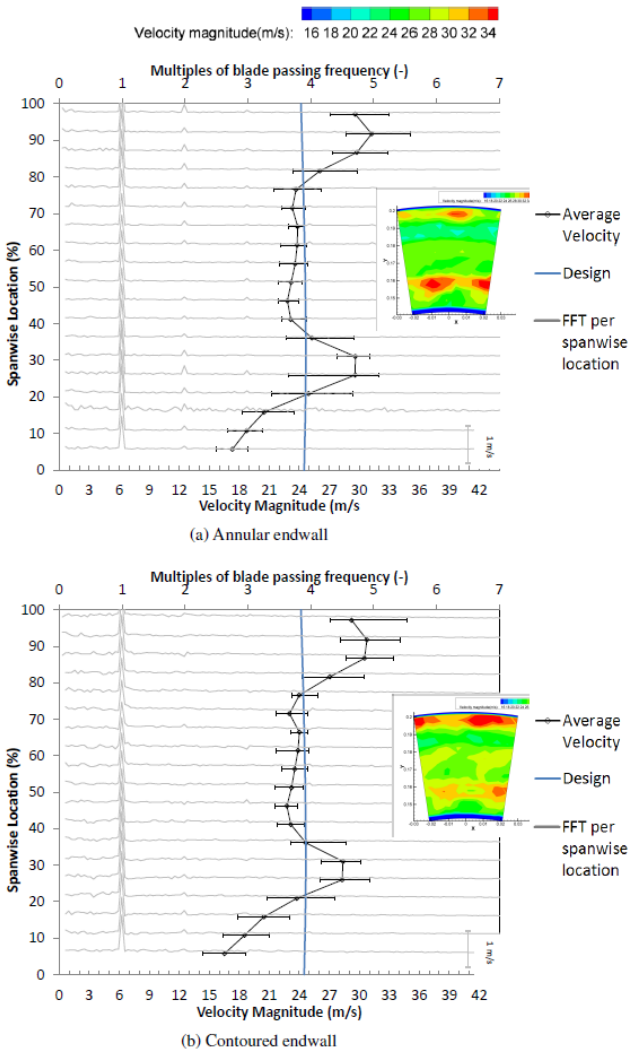

Figure 4 Design loading case: comparison of time averaged velocity magnitude downstream of the rotor.

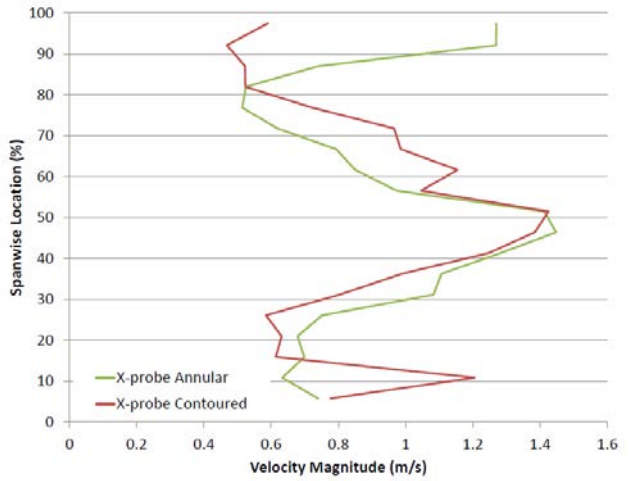

Figure 5 Design loading case: comparison of annular and contoured FFT magnitude at the blade passing frequency

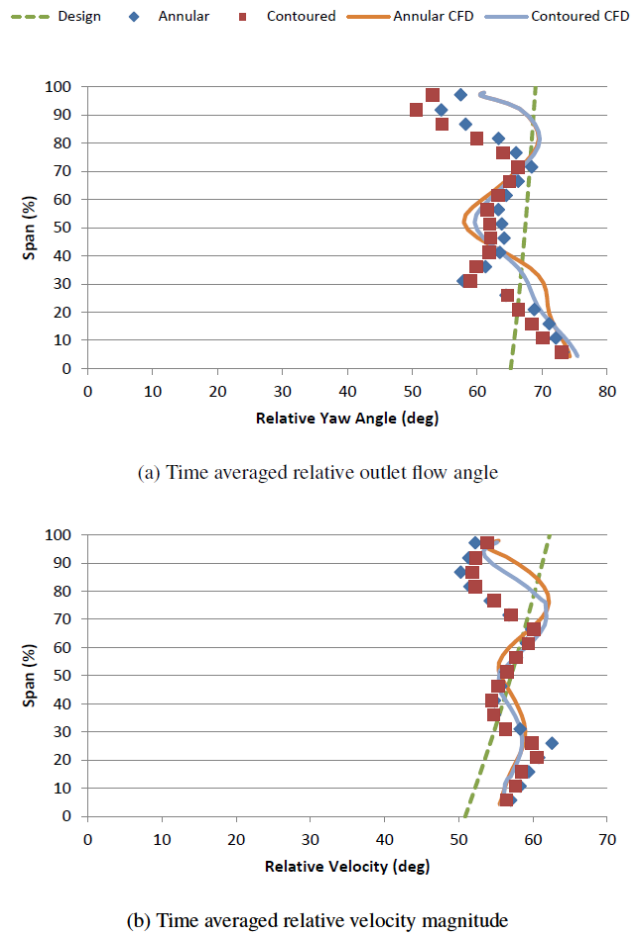

Figure 6 Design loading case: comparison of annular and contoured CFD and experimental results.

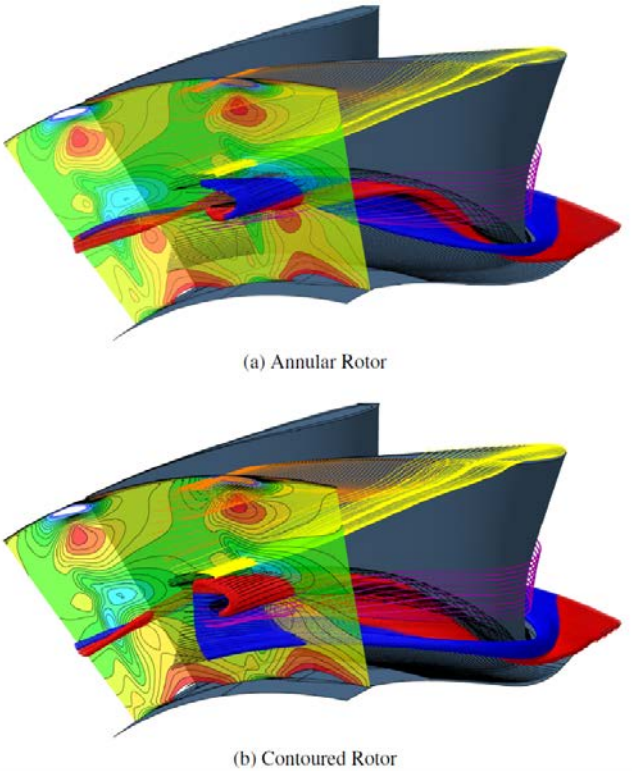

Figure 7 Design loading case: stream tubes showing the time averaged rotor exit relative outlet flow

The FFT magnitudes in figure 8 at the blade passing frequency show that there was an increase in the velocity magnitude below midspan. The contour plots shown in figure 8 show that the contoured hub endwall secondary flow vortex core was less tangentially distributed than the annular case, making the wake more pronounced causing a larger FFT magnitude at the blade passing frequency.

As was seen in the design loading case, regions of high shear were not well captured numerically. It was thought that this was in part due to difficulty in resolving the high sheared tip leakage flow, and discrepancies in component dimensions in the experimental setup to that which was modelled numerically (for instance uncertainty in manufactured components). Further research into these reasons is ongoing.

5.3 Decreased Loading Condition

Figure 11 shows the decreased loading case which shows a similar trend to the design case, with the peak velocity magnitude reduced from 29.6 m/s to 28.3 m/s in the hub endwall secondary flow region. The peak value was shifted closer to the hub endwall. Flow oscillations were reduced, specifically at 26% span. The experimental tip leakage flow was again altered by the contour, but the peak velocity magnitude remained approximately the same.

Even though the FFT magnitudes were affected the maximum change was only 0.29 m/s or 1.7× the uncertainty of the probe, thus nothing could be concluded. The magnitude of the harmonics of the blade passing frequency exhibit some differences as well, but again the magnitude oscillated about the measurement uncertainty and thus nothing can be concluded.

The numerical results of the annular and contoured rotor for the decreased loading condition showed negligible differences, as shown in figure 12.

6 Discussion

Looking at both the numerical and the experimental results it can be seen that the endwall contour has improved the rotor exit flow field, producing a more uniform velocity profile that was more aligned with the design velocity profile. The numerical investigation showed that this was due to the hub endwall secondary flow passage vortex being less tightly wrapped for the contoured case due to the reduced cross passage pressure gradient as intended by the design [2].

In general when looking at the endwall secondary flow vortex structure at 31% it can be seen that the velocity components were all reduced in magnitude, with the exception of the tangential velocity of the decreased loading case. The decreased loading tangential velocity showed an increase, but the magnitude was small enough to consider it negligible. The oscillations in the velocity was similarly reduced, as shown by the reduced FFT magnitudes at the blade passing frequency. Due to mass flow rate being fixed at the inlet of the rig this means that the peak flow was redistributed producing a more uniform outlet velocity profile.

Looking at the vortex cores in figure 7 and 13 this can be seen as a less tightly wrapped vortex (red and blue stream tubes) apparent in the contoured case compared to the annular case. Variation in the velocity profile will create fluctuations in the incidence angle experience by the downstream blade rows. Japikse [23] states that this changes the lift profile of the blade and thus results in a fluctuating blade load, which could induce the onset of blade flutter. However this would be more applicable to compressor blades as turbine blades are typically much sturdier.

When comparing all the loading conditions together, it's evident that as the loading increases so too does the effectiveness of the endwall contour (by reducing the strength of the flow in the vortex core). In light of this it is felt that designing the endwall contour for a decreased loading condition would provide a more efficient endwall design, magnifying any gains found.

Unlike that seen in the steady state experiments, the unsteady numerical tip leakage flow showed negligible differences between the annular and contoured rotor. The unsteady experimental results show a difference between the annular and contoured cases but Dunn *et al.* [24] noted that this could be due to flexure of the trailing edge of the turbine blade which was a laser sintered plastic.

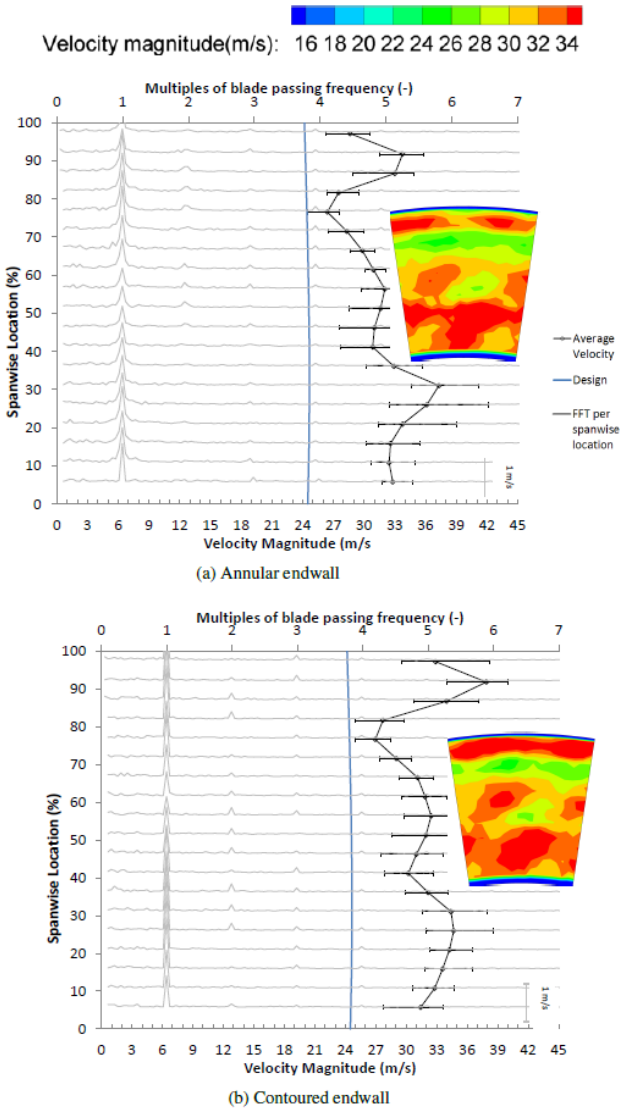

Figure 8 Increased loading case: comparison of time averaged velocity magnitude downstream of the rotor

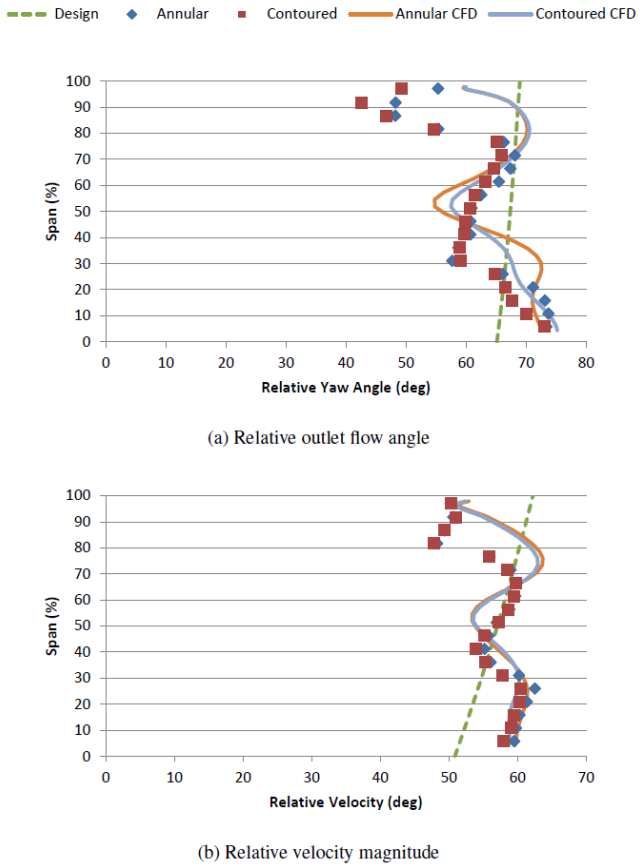

(a) Relative outlet flow angle

(b) Relative velocity magnitude

Figure 9 Increased loading case: comparison of annular and contoured CFD and experimental results

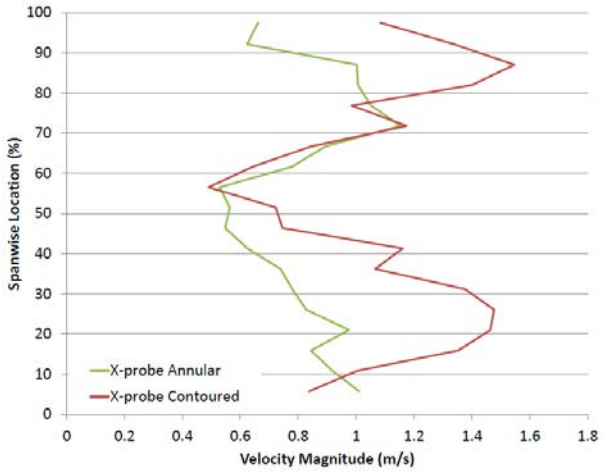

Figure 10 Increased loading case: comparison of annular and contoured FFT magnitude at the blade passing frequency

In regions of high shear the numerical results did not predict the rotor exit flow field as well as hoped. Schobeiri *et al.* [25] commented that this was due to turbulence models still being unable to adequately predict the turbulent aspects in a turbine. The unsteady experimental results however showed a larger tip leakage vortex than the numerical results. The annular and contoured experimental results also showed some discrepancies, with the contoured rotor having more over turning of the flow. It was found that the primary cause for this was a larger than expected tip gap due to manufacturing uncertainties in the test rig shroud and the blades. This however does not impact on the results of the secondary flow at the hub. The impact of an increased tip gap will be evaluated in future works.

For all loading cases the difference between the numerical and experimental results exceeded that of the annular and contoured rotor. The implication of this is that when optimising the endwall design great care should be used when choosing an objective function.

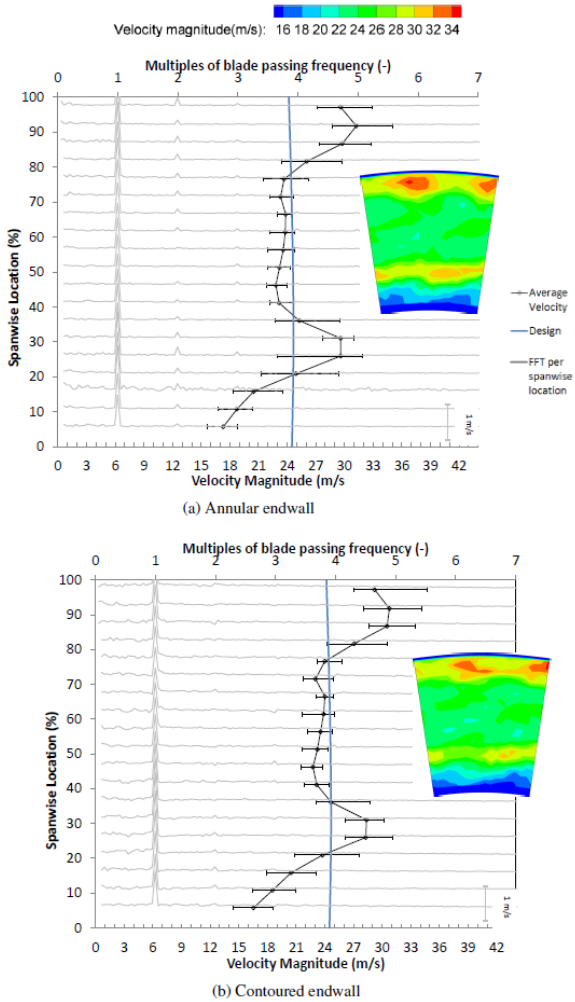

(a) Annular endwall

(b) Contoured endwall

Figure 11 Decreased loading case: comparison of velocity magnitude downstream of the rotor

7 Conclusions

In general it was found that the addition of the endwall contours did not introduce any unsteady effects to the loading cases studied. The rotor exit flow was made to be more uniform and closer to the design intent of the turbine, with a weaker endwall secondary flow vortex system. The following were concluded from the results:

1. A generic endwall contour designed for a 2D cascade improved the rotor exit flow in a rotating test rig.
2. The hub endwall secondary flow vortex system was reduced in strength, redistributing the high momentum core in the radial direction. This produces a more uniform downstream blade inlet velocity profile.

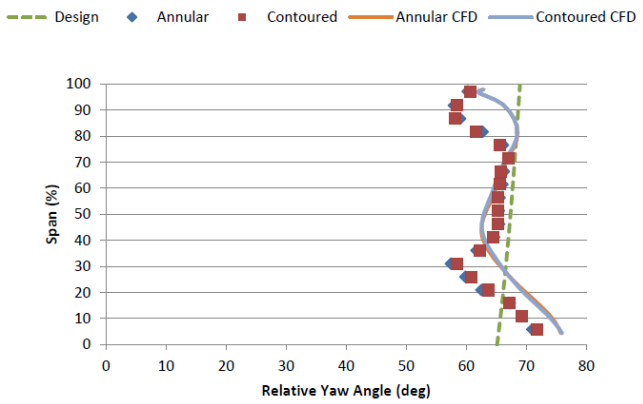

(a) Relative outlet flow angle

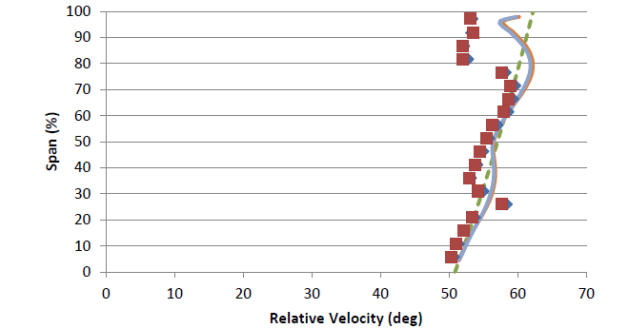

(b) Relative velocity magnitude

Figure 12 Decreased loading case: comparison of annular and contoured CFD and experimental results

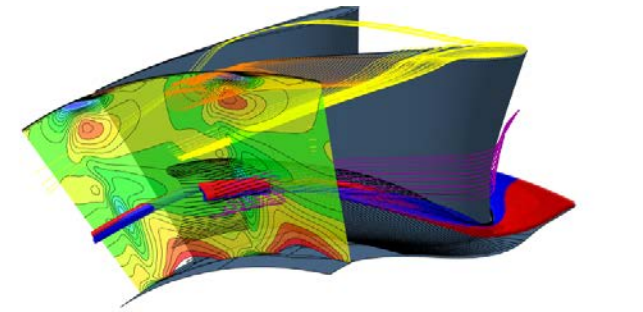

(a) Annular Rotor

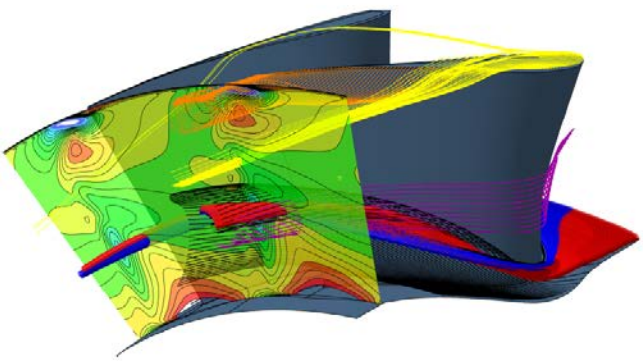

(b) Contoured Rotor

Figure 13 Decreased loading case: stream tubes showing the rotor exit relative outlet flow

3. The oscillations in the flow were reduced due to the redistribution of the hub endwall secondary flow vortex in the radial direction. The redistribution reduced the peak to peak magnitude resulting in a lower incidence angle variation experienced by the downstream blade rows.
4. A generic hub endwall contour designed for a linear cascade has not introduced any new unsteady effects to the rotor exit flow of an annular rotating test rig, even at off design conditions.
5. The effectiveness of the endwall contour increases with an increase in loading. Designing the endwall contour for an unloaded case will produce a larger performance increase at the design condition.

References

[1] M. G. Rose. Non-axisymmetric endwall profiling in the HP NGV's of an axial flow gas turbine. In *ASME 94-GT-249*, 1994.

[2] G. L. Ingram. *Endwall Profiling for the Reduction of Secondary Flow in Turbines*. PhD thesis, Durham University, 2003.

[3] G. Snedden, D. Dunn, G. Ingram, and D. Gregory-Smith. The performance of a generic nonaxisymmetric end wall in a single stage, rotating turbine at on and off-design conditions. In *ASME Turbo Expo 2010: Power for Land Sea and Air*, pages 1069-1080, 2010.

[4] P. Marchal, and C. H. Sieverding. Secondary flows within turbomachine bladings. In *AGARD Secondary Flows in Turbomachines*, 1977.

[5] H. P. Hodson, and R. G. Dominy. Three-dimensional flow in a low pressure turbine cascade at its design condition. *Journal of Turbomachinery*, 109(2):177–185, 1987.

[6] D. Gregory-Smith, G. Ingram, P. Jayaraman, N. W. Harvey, and M. G. Rose. Non-axisymmetric turbine end wall profiling. *Proceedings of the Institution of Mechanical Engineers, Part A: Journal of Power and Energy*, 215(6):721–734, 2001.

[7] N. W. Harvey, G. Brennan, D. A. Newman, and M. G. Rose. Improving turbine efficiency using non-axisymmetric endwalls: Validation in the multi-row environment and with low aspect ratio blading. In *ASME Turbo Expo 2002: Power for Land, Sea, and Air*, pages 119-126, 2002.

[8] A. E. Mensch, and K. A. Thole. Effects of non-axisymmetric endwall contouring and film cooling on the passage flowfield in a linear turbine cascade. *Experiments in Fluids*, 57(1):1–16, 2016.

[9] M. Rezasoltani, M. T. Schobeiri, and J. C. Han. Experimental investigation of the effect of purge flow on film cooling effectiveness on a rotating turbine with nonaxisymmetric end wall contouring. *Journal of Turbomachinery*, 136(9):091009, 2014.

[10] M. T. Schobeiri, K. Lu, and M. Rezasoltani. Effect of non-axisymmetric contouring on performance and film cooling of a rotating turbine endwall subjected to the secondary air purge: A combined numerical and experimental study. *Proceedings of the Institution of*

Mechanical Engineers, Part A: Journal of Power and Energy, 229(8):813–831, 2015.

[11] G. C. Snedden. *The Application of Non-Axisymmetric Endwall Contouring in a 1.5 Stage, Rotating Turbine*. PhD thesis, School of Engineering, Durham University, 2011.

[12] D. I. Dunn, G. Snedden, T. W. von Backström, and M. P. Mdluli. Unsteady effects of a generic non-axisymmetric endwall contour on the rotor of a 1½ stage low speed turbine test rig. In *ASME Turbo Expo 2013: Turbine Technical Conference and Exposition*, GT2013-94961, 2013.

[13] G. Ingram, D. Gregory-Smith, and N. Harvey. Experimental quantification of the benefits of end-wall profiling in a turbine cascade. In *ISABE 2003*, 2003.

[14] NREC. *The design and performance analysis of axial-flow turbines: Volumes I and II*. Northern Research and Engineering Corporation, 1972.

[15] G. C. Snedden, T. H. Roos, D. I. Dunn, and D. Gregory-Smith. Characterisation of a refurbished 1½ stage turbine test rig for flowfield mapping behind blading with non-axisymmetric contoured endwalls. In *ISABE 2007*, 2007.

[16] B. Perlman, and V. Auerbach. A phase-locking technique for estimating the ensemble average of time-series data. *IEEE Transactions on Acoustics, Speech and Signal Processing*, 25(4):295–299, 1977.

[17] H. D. Joslyn, R. P. Dring, and O. P. Sharma. Unsteady three-dimensional turbine aerodynamics. *Journal of Engineering for Power*, 105(2):322–331, 1983.

[18] D. I. Dunn, G. C. Snedden, and T. W. von Backström. Turbulence model comparisons for a low pressure 1.5 stage test turbine. In *ISABE 2009*, 2009.

[19] G. C. Snedden, D. I. Dunn, G. Ingram, and T. W. von Backström. Observations on the selection of objective function for the optimisation of turbine endwalls using computational fluid dynamics. In *SACAM10, South African Association for Theoretical and Applied Mechanics*, January, 2010.

[20] D. I. Dunn, G. C. Snedden, and T. W. von Backström. Numerical investigation into the unsteady effects of non-axisymmetric turbine endwall contouring on secondary flows. In *ISABE 2011*, 2011.

[21] Numeca. *User Manual FINE/Turbo v8 (including Euranus) Documentation v8a*. Numeca International, Brussels, Belgium, v8a edition, 2007.

[22] D. I. Dunn. *The Effect of Endwall Contouring on the Unsteady Flow through a Turbine Rotor*. PhD thesis, Department of Mechanical and Mechatronic Engineering, Stellenbosch University, 2014.

[23] D. Japikse. *Advanced Topics in Turbomachinery Technology, Principal Lecture Series No. 2*. Concepts ETI, Norwich, Vermont, USA, 1986.

[24] D. I. Dunn, G. C. Snedden, and T. W. von Backström. Unsteady effects of a generic non-axisymmetric rotor endwall contour on a 1½ stage turbine test rig at off design conditions. In *ASME Turbo Expo 2014: Turbine Technical Conference and Exposition*, June, 2014.

[25] M. T. Schobeiri, S. Abdelfattah, and H. Chibli. Investigating the cause of computational fluid dynamics deficiencies in accurately predicting the efficiency and performance of high pressure turbines: A combined experimental and numerical study. *Journal of Fluids Engineering*, 134(10):1–12, 2012.

